This Number Completes Volume 191
Volume 191, Number 3, September 2015

ISSN 1047-8477

Journal of Structural Biology

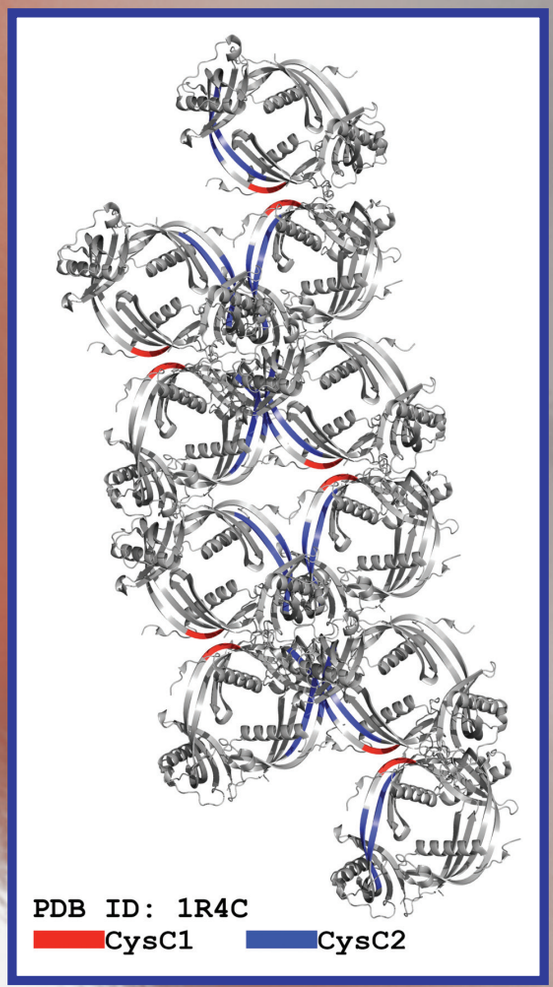

Available online at www.sciencedirect.com

ScienceDirect

Journal of Structural Biology 191 (2015) 272–280

Contents lists available at ScienceDirect

Journal of Structural Biology

journal homepage: www.elsevier.com/locate/yjsbi

Exploring the 'aggregation-prone' core of human Cystatin C: A structural study

Paraskevi L. Tsiolaki, Nikolaos N. Louros, Stavros J. Hamodrakas, Vassiliki A. Iconomidou *

Department of Cell Biology and Biophysics, Faculty of Biology, University of Athens, Panepistimiopolis, Athens 157 01, Greece

ARTICLE INFO

Article history:
Received 8 May 2015
Received in revised form 21 July 2015
Accepted 30 July 2015
Available online 31 July 2015

Keywords:
Human Cystatin C
Hereditary Cystatin C Amyloid Angiopathy
Stefin
3D-domain swapping
'Aggregation-prone' peptides
Amyloid fibrils

ABSTRACT

Amyloidogenic proteins like human Cystatin C (hCC) have been shown to form dimers and oligomers by exchange of subdomains of the monomeric proteins. Normally, the hCC monomer, a low molecular type 2 Cystatin, consists of 120 amino acid residues and functions as an inhibitor of cysteine proteases. The oligomerization of hCC is involved in the pathophysiology of a rare form of amyloidosis namely Icelandic hereditary cerebral amyloid angiopathy, in which an L68Q mutant is deposited as amyloid in brain arteries of young adults. In order to find the shortest stretch responsible to drive the fibril formation of hCC, we have previously demonstrated that the LQVVR peptide forms amyloid fibrils, *in vitro* (Tsiolaki et al., 2015). Predictions by AMYLPRED, an amyloidogenic determinant prediction algorithm developed in our lab, led us to synthesize and experimentally study two additional predicted peptides derived from hCC. Along with our previous findings, in this work, we reveal that these peptides self-assemble, in a similar way, into amyloid-like fibrils *in vitro*, as electron microscopy, X-ray fiber diffraction, ATR FT-IR spectroscopy and Congo red staining studies have shown. Further to our experimental results, all three peptides seem to have a fundamental contribution in forming the "aggregation-prone" core of human Cystatin C.

1. Introduction

Under appropriate conditions, proteins or peptides undergo conformational changes leading from their soluble forms into ordered fibrillar aggregates, called amyloid fibrils. To date, 30 different proteins can form amyloids and although there is no apparent homology in their primary sequence or their 3D structure, they do share the propensity to self-assemble and form insoluble fibrils. The pathological consequences of the formation of amyloid fibrils are implicated in a wide range of divergent neurodegenerative diseases such as Alzheimer's, Parkinson's, Creutzfeldt-Jacob's and Huntington's disease and many more, known as amyloidoses (Sipe et al., 2012).

Human Cystatin C (hCC), a 120-aminoacid protein (Fig. 1A) (Abrahamson et al., 1987), belongs to the Cystatin super-family (Barrett, 1986; Turk and Bode, 1991) and is a secretory type 2 Cystatin, expressed in all nucleated human cells (Abrahamson et al., 1986; Grubb, 2000). It is found in all tissues and body fluids (Abrahamson et al., 1986) and it is present at particularly high concentrations in cerebrospinal fluid (Abrahamson et al., 1987; Grubb and Lofberg, 1982).

hCC, belonging to the papain (C1) and legumain (C13) families (Grubb, 2000; Henskens et al., 1996; Turk and Bode, 1991), can normally inhibit cysteine proteases by an ideal binding epitope resulting from the characteristic Cystatin fold (Fig. 1B). This conformation is composed of a polypeptide that folds into a five-stranded β-sheet (β1 to β5 β-strands), which partially wraps around a central α-helix (α1 helix). The N-terminal segment and the two hairpin loops L1 and L2 build the edge of the protein, which binds into the active site of cysteine proteases and blocks their proteolytic activity (Bode et al., 1988) (Fig. 1B, Supplementary Fig. S1). In 2010, Koladziejczyk et al., created a monomer-stabilized human Cystatin C with an engineered disulfide bond [(L47C)-(G69C)] (Kolodziejczyk et al., 2010) and revealed for the first time the canonical structure features of hCC (Supplementary Fig. S1).

Aggregation and oligomerization of hCC accelerates a rare form of amyloidosis, called Hereditary Cystatin C Cerebral Amyloid Angiopathy (Icelandic Cerebral Angiopathy, HCCAA) (Gudmundsson et al., 1972). This angiopathy is an autosomal

Abbreviations: hCC, human Cystatin C; HCCAA, Hereditary Cystatin C Amyloid Angiopathy; ATR FT-IR spectroscopy, attenuated total reflectance Fourier-transform spectroscopy.

* Corresponding author.
E-mail addresses: etsiolaki@biol.uoa.gr (P.L. Tsiolaki), nlouros@biol.uoa.gr (N.N. Louros), shamodr@biol.uoa.gr (S.J. Hamodrakas), veconom@biol.uoa.gr (V.A. Iconomidou).

http://dx.doi.org/10.1016/j.jsb.2015.07.013
1047-8477/

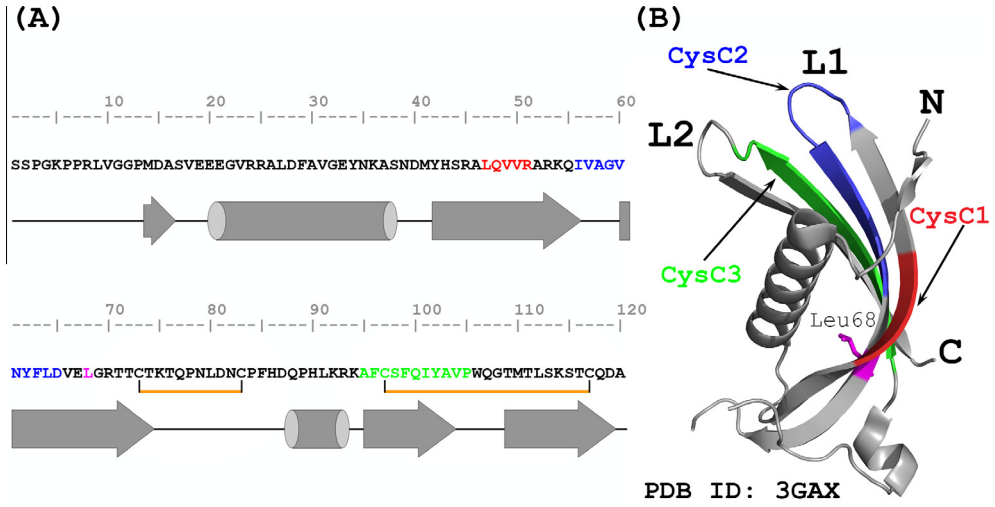

Fig. 1. Amino acid sequence and native structure of human Cystatin C (hCC). (A) A representation of the polypeptide sequence of human Cystatin C, which normally consists of 120 amino acid residues (Grubb, 2000). Predicted 'aggregation-prone' segments by AMYLPRED (Frousios et al., 2009), are shown in red (^{47}LQVVR^{51}), blue (^{56}IVAGVNYFLD^{65}) and green (^{95}AFCSQIYAVP^{105}), respectively. Dark yellow lines point out existing disulfide bonds. (B) A monomer-stabilized human Cystatin C with an engineered disulfide bond (PDB ID: 3GAX) (Kolodziejczyk et al., 2010) reveals the canonical Cystatin fold, based on the crystal structure of chicken Cystatin (Bode et al., 1988). Colored regions in red, blue and green, illustrate the *CysC1* (^{47}LQVVR^{51}), *CysC2* (^{56}IVAGVNYFLD^{65}) and *CysC3* (^{95}AFCSFQIYAVP^{105}) 'aggregation-prone' segments, respectively. The magenta region, presented as sticks, highlights a naturally occurring mutant of hCC at position 68 (L68Q). (N: N-terminal, C: C-terminal, L1: loop 1, L2: loop 2).

dominant disorder which forms amyloid deposits in brain arteries of young adults mainly originating from Iceland, leading to fatal cerebral hemorrhage (Asgeirsson et al., 1998; Olafsson and Grubb, 2000). Simultaneously, under denaturing conditions amyloid deposits of hCC are found in the leptomeninges, cerebral cortex and brainstem of older adults (Revesz et al., 2009). In addition to amyloidosis, it was demonstrated that human Cystatin C is co-deposited in the amyloid plaques of Alzheimer's disease (Levy et al., 2001) and Down's syndrome (Zerovnik, 2009) and it is also involved in tissue-degenerative diseases such as osteoporosis and periodontitis (Johansson et al., 2000).

Several crystal structures of human Cystatin C have been reported, but in all of them the protein exists in the form of symmetric three-dimensional, domain-swapped dimers (Janowski et al., 2004; Janowski et al., 2005; Janowski et al., 2001). Three-dimensional domain swapping (3D domain swapping), as a mechanism, requires partial unfolding of the monomer and subsequently separation of the exchanged domains in order to recombine and lead to the formation of an oligomer (Bennett et al., 1995; Liu and Eisenberg, 2002). A naturally occurring mutant of hCC substitutes a leucine to glutamine at position 68 (L68Q) and increases the propensity for amyloid formation through 3D domain swapping, since the substitution greatly affects the stability of the molecule (Rostagno et al., 2010) (Fig. 1B, Supplementary Fig. S1).

Based on this data, in order to find the shortest stretch responsible to drive the fibril formation of hCC, we extensively studied the structural properties of the predicted pentapeptide LQVVR and we demonstrated that this peptide has, on its own, the tendency to self-assemble forming amyloid-like fibrils, *in vitro* (Tsiolaki et al., 2015). Along with our previous findings, in this work, we report on the self-assembly properties of two (2) other hCC peptides and discuss the implications of our results.

2. Materials and methods

2.1. Prediction of potential aggregation prone peptides in human Cystatin C

AMYLPRED (Frousios et al., 2009), as well as AMYLPRED2 (Tsolis et al., 2013), both consensus algorithms developed in our lab, were used to identify 'aggregation-prone' segments in the amino acid sequence of human Cystatin C (Uniprot AC: P01034). Our tools, are publicly available for academic users in our website: http://biophysics.biol.uoa.gr/. In addition to the peptide segment ^{47}LQVVR^{51} (*CysC1*), which has shown to be pivotal for human Cystatin C oligomerization (Tsiolaki et al., 2015), two oligopeptides with high aggregation propensity were predicted (Supplementary Fig. S2). The decapeptide ^{56}IVAGVNYFLD^{65} (*CysC2*) and the 11-residue peptide ^{95}AFCSFQIYAVP^{105} (*CysC3*) (Fig. 1, colors) are located in the hinge loop L1 and in the β4 β-strand, respectively (see Section 1). It is well known that cysteine 97 in the sequence of human Cystatin C forms with cysteine 117 the one out of two disulfide bridges, in all type 2 Cystatins (Rawlings and Barrett, 1990).

2.2. Peptide synthesis

In case of ^{95}AFCSFQIYAVP^{105} prediction, we designed the analogue ^{95}AFASFQIYAV^{104} (*CysC3*) by replacing the cysteine 97 residue with an alanine, in order to prevent the formation of undesirable, intermolecular disulfide bonds between cysteines. Additionally we omitted the C-terminal proline residue (P105) in order not to disrupt the structure that is going to be formed. We should mention that the peptide analogue ^{95}AFASFQIYAV^{104} (*CysC3*) is also an "aggregation-prone" peptide, according to AMYLPRED prediction (data not shown). Both peptides, ^{56}IVAGVNYFLD^{65} (*CysC2*) and ^{95}AFASFQIYAV^{104} (*CysC3*), were synthesized by GeneCust Europe, Luxembourg© (purity >98%, free N and C terminals).

2.3. Formation of amyloid-like fibrils

The synthesized peptide ^{56}IVAGVNYFLD^{65} (*CysC2*) was dissolved (a) in distilled water, pH 5.5, at a concentration of 10 mg ml^{-1} and (b) in distilled water, pH 5.5, at a concentration of 5 mg ml^{-1}. In both cases this peptide analogue was found to produce gels spontaneously after its dilution. Samples for electron microscopy were collected continuously on an everyday basis for 11 days (Supplementary Fig. S3). Similarly, the synthesized peptide ^{95}AFASFQIYAV^{104} (*CysC3*) was dissolved in distilled water, pH 5.5, at a concentration of 10 mg ml^{-1} and respectively gels were

formed after 1–2 weeks of incubation. In all cases, gels contained amyloid-like fibrils which are judged to be amyloids from their tinctorial, morphological and structural characteristics (see Section 3) were formed.

2.4. X-ray diffraction

In order to produce oriented fibers from both *CysC2* and *CysC3* peptides, a droplet (5 μl) of each mature fibril suspension at a concentration of 10 mg ml^{-1} was placed between two properly aligned siliconized glass rods (~2 mm apart). Each droplet was allowed to dry slowly at ambient temperature and humidity for about 30 min to form an oriented fiber suitable for X-ray diffraction. The X-ray diffraction patterns were collected, using a SuperNova-Agilent Technologies X-ray generator equipped with a 135-mm ATLAS CCD detector and a 4-circle kappa goniometer, at the Institute of Biology, Medicinal Chemistry and Biotechnology, National Hellenic Research Foundation (CuK_α high intensity X-ray micro-focus source, λ = 1.5418 Å), operated at 50 kV, 0.8 mA. For the *CysC2* oligopeptide the specimen-to-film distance was set at 105 mm and the exposure time was set to 1800 s. For the *CysC3* peptide-analogue the specimen-to-film distance was set at 55 mm and the exposure time was set to 600 s. The X-ray patterns, were initially viewed using the program CrysAlisPro (CrysAlis^{PRO}, 2014) and consequently measured with the aid of the program iMosFLM (Leslie and Powell, 2007). Indexing (h, k, l, d_{obs}, d_{calc}) of the X-ray diffraction pattern from the *CysC2* peptide fiber was done utilizing DICVOL06 (Boultif and Louër, 2004). Model hexapeptides corresponding to fragments of CysC2 were obtained from ZipperDB (Goldschmidt et al., 2010). The model coordinates of the CysC2 hexapeptides are the result of threading them onto the NNQQNY structure backbone, and energetically evaluating them utilizing the Rosetta-Design program (Kuhlman and Baker, 2000).

2.5. Negative staining

For negative staining, *CysC2* and *CysC3* peptide solutions were independently applied to glow-discharged 400-mesh carbon-coated copper grids for approximately 60 s. The grids were stained with a drop (5 μl) of 2% (w/v) aqueous uranyl acetate for 60 s. Excess stain was removed by blotting with a filter paper and then the grids were air-dried. The fibril containing grids were examined with a Morgagni™ 268 transmission electron microscope, operated at 80 kV. Digital acquisitions were performed with an 11 Mpixel side-mounted Morada CCD camera (Soft Imaging System, Muenster, Germany).

2.6. Congo red staining and polarized light stereomicroscopy

Fibril suspensions of the two peptide solutions were applied to glass slides and were allowed to air-dry. The film produced by *CysC2* was stained with a 1% Congo red solution in distilled water (pH 5.75) at room temperature for approximately 20 min, as indicated by the Romhanyi protocol published in 1971 and excess stain was removed through tap water washes (Bely and Makovitzky, 2006; Romhanyi, 1971). The film formed by the *CysC3* was stained with a 10 mM Congo red solution in phosphate-buffered saline (pH 7.4) for approximately 1 h (Divry and Florkin, 1927). Excess staining was removed by several washes with 90% ethanol and left to dry at room temperature. Subsequently, the samples were observed under bright field illumination and between crossed polars, using a Leica MZ75 polarizing stereomicroscope equipped with a JVC GC-X3E camera.

2.7. Attenuated total reflectance Fourier-transform infrared spectroscopy (ATR FT-IR) and post-run computations of the spectra

A drop (5 μl) of each of the hCC peptide analogues, *CysC2* and *CysC3*, mature fibril suspensions were cast on a front-coated Au mirror and left to dry slowly at ambient conditions to form thin films. Infrared spectra were obtained from these films at a resolution of 4 cm^{-1}, utilizing an IR microscope (IRScope II by Bruker Optics) equipped with a Ge attenuated total reflectance (ATR) objective lens (20×) and attached to a Fourier-transform infrared (FTIR) spectrometer (Equinox 55, by Bruker Optics). Internal reflection spectroscopy has several advantages compared with the more common KBr dispersion technique (de Jongh et al., 1996). The choice of ATR was dictated by the need to exclude any possible spectroscopic and chemical interactions between the sample and the dispersing medium. Having a penetration depth ca. 1–2 μm (1000 cm^{-1}, Ge), ATR is free of saturation effects, which may be present in the transmission spectra of thicker samples. Moreover, the use of a microscope facilitates the acquisition of data from small samples. Ten 32-scan spectra were collected from each sample and averaged to improve the S/N ratio. The spectra are shown in the absorption mode after correction for the wavelength dependence of the penetration depth (pd ~ λ). Absorption band maxima were determined from the minima in the second derivative of the corresponding spectra. Derivatives were computed analytically using routines of the Bruker OPUS/OS2 software and included smoothing by the Savitzky–Golay algorithm (Savitsky and Golay, 1964) over a ±8 cm^{-1} range, around each data point. Smoothing over narrower ranges resulted in a deterioration of the S/N ratio and did not increase the number of minima that could be determined with confidence.

2.8. Structural analysis and figure preparation

Sequence alignments were performed using CLUSTALW (Larkin et al., 2007) and were illustrated using BioEdit (Hall, 1999). Cystatin C models were built by analyzing the PDB files 3GAX (Kolodziejczyk et al., 2010), 1R4C (Janowski et al., 2004) and 1TIJ (Janowski et al., 2005). 3GAX represents the fold of monomer-stabilized Cystatin C, whereas 1R4C and 1TIJ represent 3D domain swapped human Cystatin C of an orthorhombic and a tetragonal crystal, respectively. Figures were visualized and prepared using the PyMol software (Delano, 2005).

3. Results

Both peptides, predicted by AMYLPRED (Frousios et al., 2009) as segments of human Cystatin C with high aggregation propensity (Fig. 1, Supplementary Fig. S1), were studied in detail after synthesis and were found to self-assemble into amyloid like fibrils, forming gels after incubation for 1–2 weeks, in distilled water (see Section 2.1).

3.1. CysC2 experimental results

Solutions of peptide *CysC2* (5 mg ml^{-1} and 10 mg ml^{-1}) were prepared at pH 5.5 and incubated at ambient temperature for 2 weeks.

Aliquots of the dissolved *CysC2* peptide, at a concentration of 5 mg ml^{-1}, were extracted every day and examined utilizing T.E.M. (Transmission Electron Microscopy) after negative staining. Fibrils were formed and the thinnest single fibril had a diameter of approximately 10 nm and it was observed immediately after the peptide dilution (Supplementary Fig. S3, Day0). These fibrils have the tendency to associate laterally even macroscopically on the

grid (data not shown). The discovery of these early forming species co-exists not only with fibril bundles during the first day (Day 1) of incubation but also with microcrystals approximately 20 nm in diameter (Supplementary Fig. S3). However, on the fourth day of incubation the number of microcrystals/fibrils has considerably increased. Actually, detailed observations reveal that microcrystals consist of typical amyloid-like fibrils (~10 nm, Fig. 2 thin arrow) which wound around each other and form larger helical assemblies (Supplementary Fig. S3, Day 4). As shown in Fig. 2A (thick arrows), a twisted ribbon-like microcrystal consists of coiled fibrils (~10 nm) with an axial crossover repeat of 250 nm. These helical assemblies give rise to lamellar crystals, as seen in Supplementary Fig. S3 (Day 11) (Sawaya et al., 2007).

Congo red binds to mature fibrils derived from the *CysC2* peptide, shown in the bright field panel in Fig. 2C (left) and subsequently exhibits a yellow to apple-green birefringence when placed between crossed polars (Fig. 2C, right).

The X-ray diffraction patterns of oriented fibers from *CysC2* indicate a powder-like pattern of a polycrystalline material (Fig. 2E). This can easily be explained by looking at the EM photographs of *CysC2* (Fig. 2A). Reflections appear as rings due to poor alignment of the constituent fibrils. The strong reflections

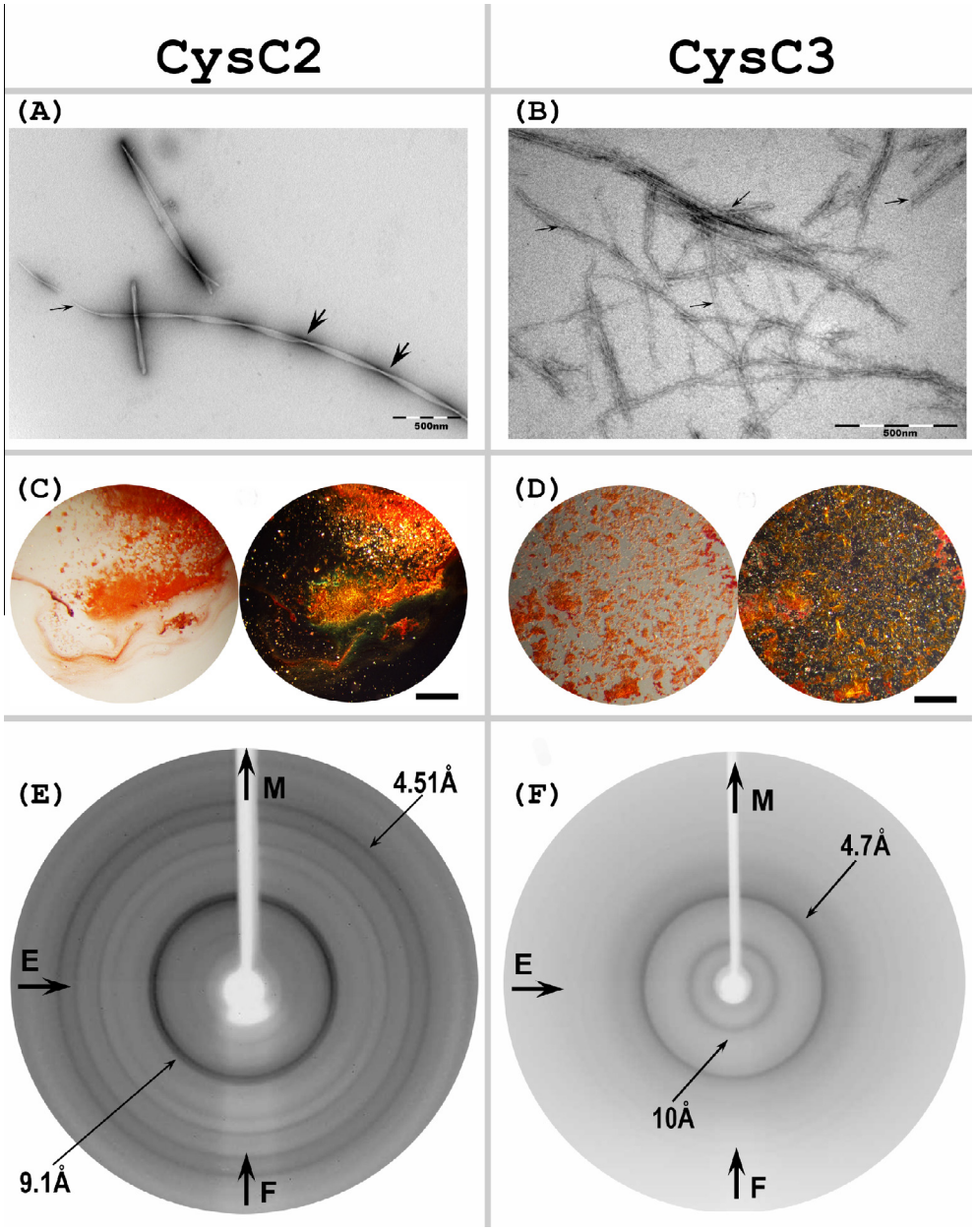

Fig. 2. Experimental results of *CysC2* and *CysC3* "aggregation-prone" peptides. (A) and (B) Electron micrographs of mature amyloid-like fibrils from CysC2 and CysC3 peptides, respectively. The samples were negatively stained with 2% uranyl acetate. Arrows show the fibrils (See Section 3). Bar 500 nm. (C) and (D) Photomicrographs of CysC2 and CysC3 peptide fibrils stained with Congo Red: bright field illumination (left), crossed polars (right). The yellow-green birefringence characteristic for amyloid fibrils is clearly seen under crossed polars (right) in both cases. Bar 500 μm. (E) and (F) X-ray diffraction patterns from oriented fibers (F) of CysC2 and CysC3 amyloid-like fibrils. In this display, the meridian, M (direction parallel to the fiber axis) is vertical and the equator, E, is horizontal. Both patterns illustrate the typical "cross-β" reflections. The 4.5–4.7 Å reflection corresponds to the spacing of adjacent beta-strands and the 9–12 Å spacing, which corresponds to the face-to-face separation (packing distance) of the β-sheets. The X-ray diffraction pattern of *CysC2* (E) is not a typical "cross-β" pattern since it shows rings instead of oriented reflections at the meridian and the equator. This indicates a random packing of the constituent amyloid fibrils in the fiber.

corresponding to periodicities of 4.51 Å and 9.14 Å may be attributed to the interstrand and inter-sheet distances of β-sheet arrangements, respectively. These reflections are characteristic of the "cross-β" conformation (Geddes et al., 1968), and are observed for several amyloid-like fibrils (Sunde and Blake, 1997), in which the β-strands are perpendicular to the fiber axis and the sheets are packed parallel to the fiber axis. A list of the reflections observed in the X-ray pattern (Fig. 2E) is given in Table 1. A full explanation of the diffraction pattern is given in the legend of Table 1, with a table of the *d*-spacings of the diffraction rings and a proposed unit cell for the polycrystalline fiber. A possible packing arrangement of *CysC2*, resulting from our indexing utilizing DICVOL06 (Boultif and Louër, 2004), illustrates the packing of the CysC2 peptide-analogue and all possible interactions between *CysC2* peptides in an orthorhombic unit cell (Fraser et al., 1965). Following the steric zipper terminology proposed by Sawaya et al., 2007, we were led to suggest a Class 7 steric zipper with an up-up arrangement (Sawaya et al., 2007) (Supplementary Fig. S4, Table 1).

An ATR FTIR spectrum of a thin film cast from suspensions of the amyloid-like fibrils of *CysC2* is shown in Fig. 3A (Table 2). The spectrum (Fig. 3A, Table 2) shows prominent bands at 1623 cm^{-1}, 1556 cm^{-1}, and 1232 cm^{-1} in the amide I, II, and III regions, respectively, indicative of a β-sheet conformation. The high wavenumber band at 1696 cm^{-1} is an indication that β-sheets are antiparallel, whilst the sharp maximum peak at 1515 cm^{-1} is typically assigned to Tyr (Y) (C—C stretching vibration of the aromatic ring) (Haris and Chapman, 1995; Jackson and Mantsch, 1995; Krimm and Bandekar, 1986; Surewicz et al., 1993; Tremmel et al., 2005; Valenti et al., 2011). The resulting ATR FT-IR spectrum strongly supports the presence of an antiparallel β-sheet conformation.

3.2. CysC3 experimental results

The synthesized *CysC3* peptide at a concentration of 10 mg ml^{-1} self-assembles into mature amyloid fibrils after 2 weeks of incubation in distilled water.

Electron micrographs show that they are linear unbranched fibrils of indeterminate length and uniform in diameter (ca. ~10 nm, arrows). They tend to aggregate laterally ("side by side") and in register (Fig. 2B, thin arrows), forming bundles of fibrils.

These fibrils bind Congo red (Fig. 2D, left) showing the characteristic yellow-green birefringence when seen under crossed polars (Fig. 2D, right). In addition, X-ray diffraction patterns from fibers

Table 1
Spacings (d_{obs}) of the reflections that were observed in the X-ray diffraction pattern, taken from a fiber of the *CysC2* peptide amyloid-like fibrils (Fig. 2, Supplementary Fig. S4). Indexing (*h*, *k*, *l*, d_{obs}, d_{calc}) was done, utilizing DICVOL06 (Boultif and Louër, 2004), a software for the automatic indexing of powder diffraction patterns by the successive dichotomy method, based on an orthorhombic unit cell, with unit cell parameters: $a = 8.98 \pm 0.02$ Å, $b = 36.23 \pm 0.01$ Å, $c = 18.16 \pm 0.01$ Å, $\alpha = 90°$, $\beta = 90°$, $\gamma = 90°$.

h	*k*	*l*	d_{obs} (Å)	d_{calc} (Å)
0	0	2	9.14	9.13
1	3	0	7.24	7.24
0	0	3	6.07	6.08
1	0	3	5.04	5.04
2	0	0	4.51	4.50
2	2	2	3.94	3.94
2	0	3	3.61	3.62
1	10	1	3.31	3.31
1	5	5	3.06	3.06

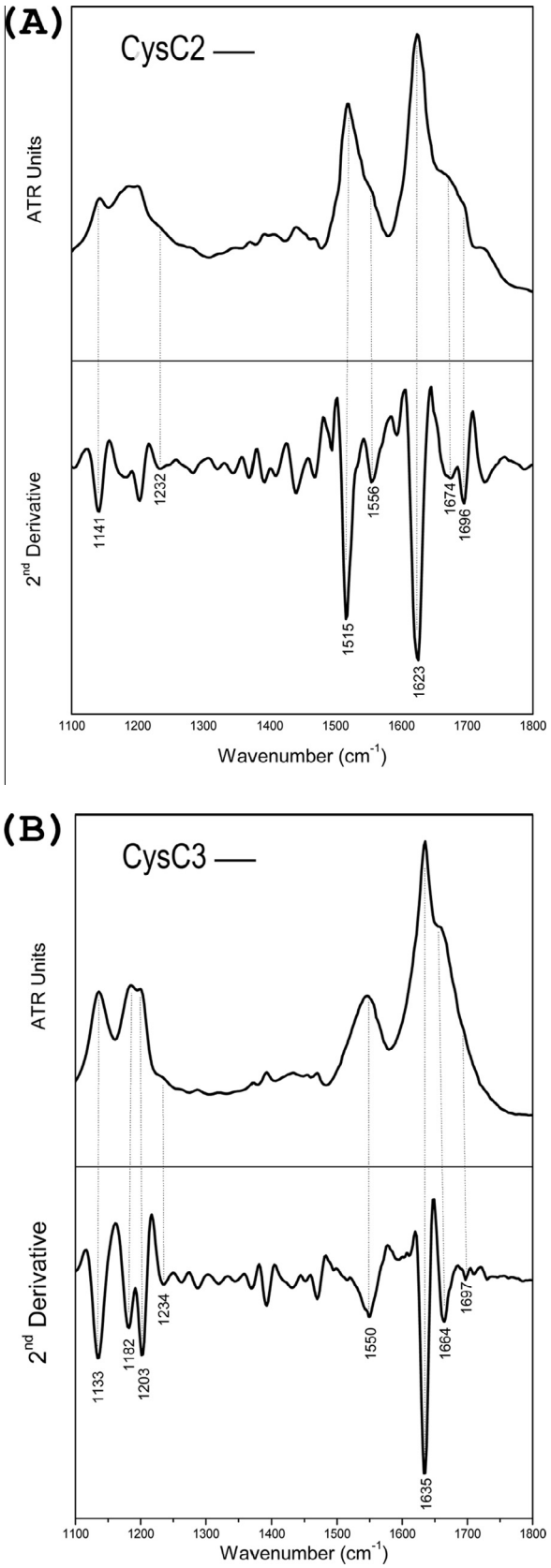

Fig. 3. ATR FT-IR (1100–1800 cm^{-1}) spectra, obtained from suspensions of fibrils, produced from the CysC2 (A) and CysC3 (B) peptides, cast on a flat stainless-steel plate and left to air-dry slowly, at ambient conditions, to form hydrated, thin films. Second derivative spectra are also included.

Table 2
Bands observed in the ATR FT-IR spectra obtained from thin-films, containing suspensions of fibrils, produced by the *CysC2* Peptide and *CysC3* peptides, respectively, and their tentative assignments.

CysC2		*CysC3*	
Band (cm^{-1})	Assignments	Band (cm^{-1})	Assignments
1141	TFA	1133, 1182, 1203	TFA
1232	Amide III (β-sheet)	1234	Amide III (β-sheet)
1515	Tyrosine side chain		
1556	Amide II (β-sheet)	1550	Amide II (β-sheet)
1623	Amide I (β-sheet)	1635	Amide I (β-sheet)
1674	TFA	1664	TFA
1696	Antiparallel β-sheet	1697	Antiparallel β-sheet

For details see text.

formed from *CysC3* peptide fibrils show two strong reflections at 4.7 Å and 10 Å (Fig. 2F). These reflections appear as rings due to the poor alignment of the constituent fibrils. This is probably due to random packing of the fibrils, which adopt all possible orientations in the fiber. The strong reflection at 4.7 Å suggests that β-sheets are present and may be attributed to inter-strand distances. The weaker reflection at ~10 Å, most probably, corresponds to inter-sheet packing distances. These two reflections clearly indicate the existence of β-sheets and are characteristic of a cross-β-like conformation observed for several amyloid-like fibrils (Fig. 2B), not oriented, however, in this case.

The ATR FT-IR spectrum from thin films produced by the *CysC3* peptide fibril-containing solutions (Fig. 3B, Table 2) shows a prominent band at 1635 cm^{-1} in the amide I region, which is a band clearly due to β-sheet conformation and a weak shoulder at 1697 cm^{-1}, which is an indication that the β-sheets are antiparallel (Haris and Chapman, 1995; Jackson and Mantsch, 1995; Krimm and Bandekar, 1986; Surewicz et al., 1993; Valenti et al., 2011). Thus, the results from ATR FT-IR spectroscopy strongly support the evidence from X-ray diffraction.

4. Discussion

By its very definition the "amyloid stretch hypothesis" proposed that amyloid aggregation is actually driven by short fragments of misfolded proteins (Esteras-Chopo et al., 2005), and thus until today, scientists in structural biology have extensively been studying a great variety of amyloidogenic (or 'aggrega tion-prone') peptides (Iconomidou et al., 2013; Iconomidou et al., 2012; Louros et al., 2014; Teng and Eisenberg, 2009; Tenidis et al., 2000). These short amyloidogenic stretches of five or six amino acid residues do exhibit the potential to 'guide' amyloid fibril formation from a soluble globular domain (Lopez de la Paz and Serrano, 2004; Teng and Eisenberg, 2009). Therefore, several published algorithms during the last decade or so, based on various properties of polypeptide chains, attempt to predict such 'aggrega tion-prone' stretches. A relatively recent review of available software was published by Hamodrakas (2011).

Utilizing our consensus prediction algorithm of 'aggrega tion-prone' segments AMYLPRED (Frousios et al., 2009), three (3) peptides of hCC were predicted as 'aggregation-prone' segments; the pentapeptide ^{47}LQVVR^{51} (*CysC1*) and the peptides ^{56}IVAGVNYFLD^{65} (*CysC2*) and ^{95}AFCSFQIYAVP^{105} (*CysC3*) (Fig. 1). Initially the LQVVR peptide was shown to have amyloidogenic properties and plays a crucial structural role in hCC fibrillation (Tsiolaki et al., 2015). In this work, we attempted to shed light on the two additional, predicted 'aggregation-prone' regions, the peptides *CysC2* and *CysC3*, and find out whether they intrinsically exhibit amyloidogenicity. Our experimental work clearly shows that twisted microcrystals formed from *CysC2* peptide solutions and fibrils formed from *CysC3* peptide solutions fulfill-in general-all three basic criteria of amyloid fibrils (see Section 3).

Several studies have reported undeniable similarities between a crystal and a fiber (Diaz-Avalos et al., 2003; Sawaya et al., 2007) and according to Marshall et al. a concrete concentration can drive the structural rearrangement of a fiber to finally form a crystal (Marshall et al., 2010). In fact, the crystals are nano-crystals with a thickness of approximately 200 nm which adopt a needle-shaped morphology (Nelson et al., 2005; Sawaya et al., 2007). In our case electron micrographs showed that the peptide *CysC2*, which consists of 10 amino acids, follows *in vitro* an assembly pathway where thin, single fibrils transform into lamellar nano-crystals within 10 days after dilution (Supplementary Fig. S3).

Besides electron micrographs, microcrystal structures are related to the diffraction patterns derived from samples derived from peptide *CysC2*. Our findings indicate a powder-like pattern of a polycrystalline material. Thus, except for the two diffraction spacings, which mainly correspond to the cross-β conformation, the diffraction spacings listed in Table 1 are thought to arise from the polycrystalline state of the samples from the peptide *CysC2* (Supplementary Fig. S4). According to Sawaya et al., both peptides and microcrystals share common principal structure features and result in producing similar diffraction patterns (Sawaya et al., 2007).

A theoretical approach to a dataset of 12 amyloidogenic proteins has shown that segments with high aggregation propensity are usually exposed on the surface of the amyloidogenic proteins (Frousios et al., 2009). In a similar way, an intriguing finding of a computational analysis by Castillo and Ventura revealed that in the homo-oligomeric form of amyloidogenic proteins, protein–protein interactions and aggregation-prone segments of the surface overlap (Castillo and Ventura, 2009).

As we have previously demonstrated, *CysC1* is both a Cystatin C-peptide with high aggregation propensity and, also, a crystal contact (Janin, 1997; Janowski et al., 2004; Tsiolaki et al., 2015). What is especially interesting is that adjacent tetramers interact through the *CysC1* peptide not only in the orthorhombic crystal (PDB ID: 1R4C) (Janowski et al., 2004) but also in the tetragonal crystal (PDB ID: 1TIJ) (Janowski et al., 2005) (Supplementary Fig. S5). However, the overall shape of 1TIJ structure stresses the high plasticity capability of the hinge loop (L1 loop, see Section 1).

Similarly, *CysC2*, which contains the L1 loop, takes part in intermolecular interactions by stabilizing the long β-sheet between Cystatin C dimers and by forming a rich network of interactions of symmetry-related molecules (Janowski et al., 2004; Janowski et al., 2005). Remarkably, except from the 'native-fold' interactions between dimers, we are able to point out the significance of the intramolecular interactions between neighboring higher oligomers-such as octamers-, utilizing the information given by the Cystatin C crystal packing (Supplementary Fig. S6). Unlike its tetragonal form (PDB ID: 1TIJ), where only *CysC1* interactions occur (Janowski et al., 2005), in the orthorhombic crystal structure 1R4C repeating interactions of both *CysC1* and *CysC2* formulate a large ordered (agglomerate) aggregate (Supplementary Fig. S6).

CysC2 is of great importance: firstly, the peptide contains the L1 loop (hinge loop, see Section 1), the linker region between β-strands β2 and β3, which is essential in hCC dimerization (Szymanska et al., 2009). The corresponding dimerization leads to a conformational change. Secondly, Orlikowska et al. has shown that specific mutations in the hinge loop can control the 3D domain swapping mechanism (Orlikowska et al., 2011). The mutated amino acid Val57 is part of our amyloidogenic determinant (^{56}IVAGVNYFLD^{65}). Thirdly, additional studies have revealed that this region of the Cystatin fold is conformationally unstable,

mostly due to the Valine residue located near the top of the loop L1 (Val57 for hCC) (Abrahamson and Grubb, 1994; Nilsson et al., 2004).

Another equally important aspect is that human Cystatin C interacts with several amyloidogenic proteins such as Amyloid β (Aβ) and Serum Amyloid A (SAA). Specific interactions between Cystatin C and Aβ (Sastre et al., 2004) and Cystatin C and SAA (Bokarewa et al., 2007) had been found experimentally and, thus, had introduced two novel Cystatin C partners. Consecutive structural experiments were performed using selective proteolytic excision and high resolution mass spectrometry (Juszczyk et al., 2009; Maftei et al., 2012; Tian et al., 2007) in order to identify the crucial binding 'hotspots' both in Aβ and SAA. Surprisingly, the identified interaction site of Aβ is located in the ^{101}IYAVPWQGTMTLSKSTC^{117} hCC fragment (Juszczyk et al., 2009), whereas the identified epitope on SAA is located in ^{96}FCSFQIY^{102} fragment (Spodzieja et al., 2013; Spodzieja et al., 2012). These studies highlight the importance of *CysC3* peptide, which according to our experimental results exhibits the tendency to self assemble into amyloid-like fibrils.

Amyloidogenic proteins, which have the tendency to aggregate via 3D domain swapping, have been a major focus of interest in recent years. Interestingly, in 2008 an attempt to determine the core structure of Stefin B was performed by using hydrogen exchange and NMR (Morgan et al., 2008). Stefin B, as a member of the Cystatin superfamily, shares high sequence similarity with Cystatin C (Supplementary Fig. S7) and adopts the same general Cystatin fold (Jenko Kokalj et al., 2007). As a α/β protein, Stefin B needs a determining conformational transition, that leads to fibrillation through 3D domain swapping (Zerovnik et al., 2011).

In analogy to the model proposed by Morgan et al. (2008) we propose a hypothetical polymerization pathway, shown in Supplementary Fig. S8. We attempted to 'locate' our aggregation prone segments and propose a plausible mechanism for the formation of the amyloid fibrils formed by hCC. To our surprise, all three peptides, which have their own ability to self-assemble, according to our results, participate in the core beta structure of the model (Supplementary Fig. S8), suggesting, perhaps, an active role of *CysC1*, *CysC2* and *CysC3* in human Cystatin C aggregation and fibrillation. Importantly, Stefin B sequence analysis utilizing AMYLPRED2, indicated that the *CysC2* homolog presents high aggregation potency, in addition to the *CysC1* and *CysC3* homologs presenting lower, yet significant, aggregation propensity (data not shown). However, an important note is that human Stefins, as type 1 Cystatins, lack native disulfide bonds, in contrast to human Cystatin C (Zerovnik et al., 2010) and thus, are more prone to partial misfolding or conformational change (Grana-Montes et al., 2012). Conclusively, future experiments are essential, such as series of point mutations in full-length Cystatin C, followed by aggregation assays, in order to experimentally verify the amyloid assembly mechanism of Cystatin C and the implication of the identified CysC1, CysC2 and CysC3 'aggregation-prone' segments.

5. Conclusions

Studies of hCC are of great importance. HCC was the first protein to exhibit the 3D domain swapping mechanism, which leads to oligomers. Until recently, hCC was a protein with no experimentally determined amyloidogenic regions. Our group revealed for the first time that the ^{47}LQVVR^{51} segment of Cystatin C (CysC1) exhibits the tendency to self-assemble and, most probably, drives the fibrillization of the protein by participating in a crucial structural region (Tsiolaki et al., 2015). In this work, utilizing electron microscopy, X-ray fiber diffraction, ATR FT-IR spectroscopy and Congo red staining, we have shown that two additional 'aggregation-prone' segments of hCC, theoretically predicted by our algorithm AMYLPRED, indeed self-assemble and might be active ingredients of hCC aggregation. Based on these results and on the published models of the Cystatin superfamily (Zerovnik et al., 2011) we propose a plausible sketchy model of hCC polymerization.

Author contributions

All authors conceived and designed the experiments. PLT and NNL performed the experiments. PLT performed the analysis and wrote the paper. VAI and SJH supervised the whole project and evaluated the results. All authors have read and approve the final version of the manuscript.

Conflict of interest

The authors declare no conflicts of interest.

Acknowledgments

We thank the University of Athens for support. This research has been co-financed by the European Union (European Regional Development Fund – ERDF) and Greek national funds through the Operational Program 'Competitiveness and Entrepreneurship' of the National Strategic Reference Framework (NSRF) (Project code 11SYN-1-1230, General Secretariat for Research and Technology of the Greek Ministry of Education and Religious Affairs, Culture and Sports). We also thank our collaborator Dr. Evangelia D. Chrysina for excellent assistance with the X-ray experiments and the Institute of Biology, Medicinal Chemistry and Biotechnology at National Hellenic Research Foundation for hospitality. We also thank Dr. Georgios E. Baltatzis and Prof Efstratios S. Patsouris for excellent assistance with Transmission Electron Microscopy experiments in the Department of Pathology, at the Medical School of the University of Athens. Finally, we should like to sincerely thank the handling editor and the reviewers of this manuscript for their very useful and constructive criticism.

Appendix A. Supplementary data

Supplementary data associated with this article can be found, in the online version, at http://dx.doi.org/10.1016/j.jsb.2015.07.013.

References

Abrahamson, M., Grubb, A., 1994. Increased body temperature accelerates aggregation of the Leu-68 → Gln mutant cystatin C, the amyloid-forming protein in hereditary cystatin C amyloid angiopathy. Proc. Natl. Acad. Sci. U.S.A. 91, 1416–1420.

Abrahamson, M., Barrett, A.J., Salvesen, G., Grubb, A., 1986. Isolation of six cysteine proteinase inhibitors from human urine. Their physicochemical and enzyme kinetic properties and concentrations in biological fluids. J. Biol. Chem. 261, 11282–11289.

Abrahamson, M., Grubb, A., Olafsson, I., Lundwall, A., 1987. Molecular cloning and sequence analysis of cDNA coding for the precursor of the human cysteine proteinase inhibitor cystatin C. FEBS Lett. 216, 229–233.

Asgeirsson, B., Haebel, S., Thorsteinsson, L., Helgason, E., Gudmundsson, K.O., Gudmundsson, G., Roepstorff, P., 1998. Hereditary cystatin C amyloid angiopathy: monitoring the presence of the Leu-68 → Gln cystatin C variant in cerebrospinal fluids and monocyte cultures by MS. Biochem. J. 329 (Pt. 3), 497–503.

Barrett, A.J., 1986. The cystatins: a diverse superfamily of cysteine peptidase inhibitors. Biomed. Biochim. Acta 45, 1363–1374.

Bely, M., Makovitzky, J., 2006. Sensitivity and specificity of Congo red staining according to Romhanyi. Comparison with Puchtler's or Bennhold's methods. Acta Histochem. 108, 175–180.

Bennett, M.J., Schlunegger, M.P., Eisenberg, D., 1995. 3D domain swapping: a mechanism for oligomer assembly. Protein Sci. 4, 2455–2468.

Bode, W., Engh, R., Musil, D., Thiele, U., Huber, R., Karshikov, A., Brzin, J., Kos, J., Turk, V., 1988. The 2.0 A X-ray crystal structure of chicken egg white cystatin and its possible mode of interaction with cysteine proteinases. EMBO J. 7, 2593–2599.
Bokarewa, M., Abrahamson, M., Levshin, N., Egesten, A., Grubb, A., Dahlberg, L., Tarkowski, A., 2007. Cystatin C binds serum amyloid A, downregulating its cytokine-generating properties. J. Rheumatol. 34, 1293–1301.
Boultif, A., Louër, D., 2004. Powder pattern indexing with the dichotomy method. J. Appl. Crystallogr. 37, 724–731.
Castillo, V., Ventura, S., 2009. Amyloidogenic regions and interaction surfaces overlap in globular proteins related to conformational diseases. PLoS Comput. Biol. 5, e1000476.
CrysAlis[PRO], 2014. Agilent Technologies, pp. Software System, Version 1.171.37.31 ed. Agilent Technologies UK Ltd., Oxford, UK.
de Jongh, H.H., Goormaghtigh, E., Ruysschaert, J.M., 1996. The different molar absorptivities of the secondary structure types in the amide I region: an attenuated total reflection infrared study on globular proteins. Anal. Biochem. 242, 95–103.
Delano, W.L., 2005. The PyMOL Molecular Graphics System. DeLano Scientific LLC400, Oyster Point Blvd., Suite 213, South San Francisco, CA 94080–1918, USA.
Diaz-Avalos, R., Long, C., Fontano, E., Balbirnie, M., Grothe, R., Eisenberg, D., Caspar, D.L., 2003. Cross-beta order and diversity in nanocrystals of an amyloid-forming peptide. J. Mol. Biol. 330, 1165–1175.
Divry, D., Florkin, M., 1927. Sur les proprietes optiques de l'amyloide. Comptes Rendus de la Societe de Biologie 97, 1808–1810.
Esteras-Chopo, A., Serrano, L., Lopez de la Paz, M., 2005. The amyloid stretch hypothesis: recruiting proteins toward the dark side. Proc. Natl. Acad. Sci. U.S.A. 102, 16672–16677.
Fraser, R.D., Macrae, T.P., Stewart, F.H., Suzuki, E., 1965. Poly-L-alanylglycine. J. Mol. Biol. 11, 706–712.
Frousios, K.K., Iconomidou, V.A., Karletidi, C.M., Hamodrakas, S.J., 2009. Amyloidogenic determinants are usually not buried. BMC Struct. Biol. 9, 44.
Geddes, A.J., Parker, K.D., Atkins, E.D., Beighton, E., 1968. "Cross-beta" conformation in proteins. J. Mol. Biol. 32, 343–358.
Goldschmidt, L., Teng, P.K., Riek, R., Eisenberg, D., 2010. Identifying the amylome, proteins capable of forming amyloid-like fibrils. Proc. Natl. Acad. Sci. U.S.A. 107, 3487–3492.
Grana-Montes, R., de Groot, N.S., Castillo, V., Sancho, J., Velazquez-Campoy, A., Ventura, S., 2012. Contribution of disulfide bonds to stability, folding, and amyloid fibril formation: the PI3-SH3 domain case. Antioxid. Redox. Signal. 16, 1–15.
Grubb, A., Lofberg, H., 1982. Human gamma-trace, a basic microprotein: amino acid sequence and presence in the adenohypophysis. Proc. Natl. Acad. Sci. U.S.A. 79, 3024–3027.
Grubb, A.O., 2000. Cystatin C – properties and use as diagnostic marker. Adv. Clin. Chem. 35, 63–99.
Gudmundsson, G., Hallgrimsson, J., Jonasson, T.A., Bjarnason, O., 1972. Hereditary cerebral haemorrhage with amyloidosis. Brain 95, 387–404.
Hall, T.A., 1999. BioEdit: a user-friendly biological sequence alignment editor and analysis program for Windows 95/98/NT. Nucleic Acids Symp. Ser. 41, 95–98.
Hamodrakas, S.J., 2011. Protein aggregation and amyloid fibril formation prediction software from primary sequence: towards controlling the formation of bacterial inclusion bodies. FEBS J. 278, 2428–2435.
Haris, P.I., Chapman, D., 1995. The conformational analysis of peptides using Fourier transform IR spectroscopy. Biopolymers 37, 251–263.
Henskens, Y.M., Veerman, E.C., Nieuw Amerongen, A.V., 1996. Cystatins in health and disease. Biol. Chem. Hoppe Seyler 377, 71–86.
Iconomidou, V.A., Leontis, A., Hoenger, A., Hamodrakas, S.J., 2013. Identification of a novel 'aggregation-prone'/'amyloidogenic determinant' peptide in the sequence of the highly amyloidogenic human calcitonin. FEBS Lett. 587, 569–574.
Iconomidou, V.A., Pheida, D., Hamodraka, E.S., Antony, C., Hoenger, A., Hamodrakas, S.J., 2012. An amyloidogenic determinant in n-terminal pro-brain natriuretic peptide (nt-probnp): implications for cardiac amyloidoses. Biopolymers 98, 67–75.
Jackson, M., Mantsch, H.H., 1995. The use and misuse of FTIR spectroscopy in the determination of protein structure. Crit. Rev. Biochem. Mol. Biol. 30, 95–120.
Janin, J., 1997. Specific versus non-specific contacts in protein crystals. Nat. Struct. Biol. 4, 973–974.
Janowski, R., Abrahamson, M., Grubb, A., Jaskolski, M., 2004. Domain swapping in N-truncated human cystatin C. J. Mol. Biol. 341, 151–160.
Janowski, R., Kozak, M., Abrahamson, M., Grubb, A., Jaskolski, M., 2005. 3D domain-swapped human cystatin C with amyloid like intermolecular beta-sheets. Proteins 61, 570–578.
Janowski, R., Kozak, M., Jankowska, E., Grzonka, Z., Grubb, A., Abrahamson, M., Jaskolski, M., 2001. Human cystatin C, an amyloidogenic protein, dimerizes through three-dimensional domain swapping. Nat. Struct. Biol. 8, 316–320.
Jenko Kokalj, S., Guncar, G., Stern, I., Morgan, G., Rabzelj, S., Kenig, M., Staniforth, R.A., Waltho, J.P., Zerovnik, E., Turk, D., 2007. Essential role of proline isomerization in stefin B tetramer formation. J. Mol. Biol. 366, 1569–1579.
Johansson, L., Grubb, A., Abrahamson, M., Kasprzykowski, F., Kasprzykowska, R., Grzonka, Z., Lerner, U.H., 2000. A peptidyl derivative structurally based on the inhibitory center of cystatin C inhibits bone resorption in vitro. Bone 26, 451–459.
Juszczyk, P., Paraschiv, G., Szymanska, A., Kolodziejczyk, A.S., Rodziewicz-Motowidlo, S., Grzonka, Z., Przybylski, M., 2009. Binding epitopes and interaction structure of the neuroprotective protease inhibitor cystatin C with beta-amyloid revealed by proteolytic excision mass spectrometry and molecular docking simulation. J. Med. Chem. 52, 2420–2428.
Kolodziejczyk, R., Michalska, K., Hernandez-Santoyo, A., Wahlbom, M., Grubb, A., Jaskolski, M., 2010. Crystal structure of human cystatin C stabilized against amyloid formation. FEBS J. 277, 1726–1737.
Krimm, S., Bandekar, J., 1986. Vibrational spectroscopy and conformation of peptides, polypeptides, and proteins. Adv. Protein Chem. 38, 181–364.
Kuhlman, B., Baker, D., 2000. Native protein sequences are close to optimal for their structures. Proc. Natl. Acad. Sci. U.S.A. 97, 10383–10388.
Larkin, M.A., Blackshields, G., Brown, N.P., Chenna, R., McGettigan, P.A., McWilliam, H., Valentin, F., Wallace, I.M., Wilm, A., Lopez, R., Thompson, J.D., Gibson, T.J., Higgins, D.G., 2007. Clustal W and Clustal X version 2.0. Bioinformatics 23, 2947–2948.
Leslie, A.G.W., Powell, H.R., 2007. Processing Diffraction Data with mosflm. Springer Netherlands, Dordrecht, The Netherlands.
Levy, E., Sastre, M., Kumar, A., Gallo, G., Piccardo, P., Ghetti, B., Tagliavini, F., 2001. Codeposition of cystatin C with amyloid-beta protein in the brain of Alzheimer disease patients. J. Neuropathol. Exp. Neurol. 60, 94–104.
Liu, Y., Eisenberg, D., 2002. 3D domain swapping: as domains continue to swap. Protein Sci. 11, 1285–1299.
Lopez de la Paz, M., Serrano, L., 2004. Sequence determinants of amyloid fibril formation. Proc. Natl. Acad. Sci. U.S.A. 101, 87–92.
Louros, N.N., Iconomidou, V.A., Tsiolaki, P.L., Chrysina, E.D., Baltatzis, G.E., Patsouris, E.S., Hamodrakas, S.J., 2014. An N-terminal pro-atrial natriuretic peptide (NT-proANP) 'aggregation-prone' segment involved in isolated atrial amyloidosis. FEBS Lett. 588, 52–57.
Maftei, M., Tian, X., Manea, M., Exner, T.E., Schwanzar, D., von Arnim, C.A., Przybylski, M., 2012. Interaction structure of the complex between neuroprotective factor humanin and Alzheimer's beta-amyloid peptide revealed by affinity mass spectrometry and molecular modeling. J. Pept. Sci. 18, 373–382.
Marshall, K.E., Hicks, M.R., Williams, T.L., Hoffmann, S.V., Rodger, A., Dafforn, T.R., Serpell, L.C., 2010. Characterizing the assembly of the Sup35 yeast prion fragment, GNNQQNY: structural changes accompany a fiber-to-crystal switch. Biophys. J. 98, 330–338.
Morgan, G.J., Giannini, S., Hounslow, A.M., Craven, C.J., Zerovnik, E., Turk, V., Waltho, J.P., Staniforth, R.A., 2008. Exclusion of the native alpha-helix from the amyloid fibrils of a mixed alpha/beta protein. J. Mol. Biol. 375, 487–498.
Nelson, R., Sawaya, M.R., Balbirnie, M., Madsen, A.O., Riekel, C., Grothe, R., Eisenberg, D., 2005. Structure of the cross-beta spine of amyloid-like fibrils. Nature 435, 773–778.
Nilsson, M., Wang, X., Rodziewicz-Motowidlo, S., Janowski, R., Lindstrom, V., Onnerfjord, P., Westermark, G., Grzonka, Z., Jaskolski, M., Grubb, A., 2004. Prevention of domain swapping inhibits dimerization and amyloid fibril formation of cystatin C: use of engineered disulfide bridges, antibodies, and carboxymethylpapain to stabilize the monomeric form of cystatin C. J. Biol. Chem. 279, 24236–24245.
Olafsson, I., Grubb, A., 2000. Hereditary cystatin C amyloid angiopathy. Amyloid 7, 70–79.
Orlikowska, M., Jankowska, E., Kolodziejczyk, R., Jaskolski, M., Szymanska, A., 2011. Hinge-loop mutation can be used to control 3D domain swapping and amyloidogenesis of human cystatin C. J. Struct. Biol. 173, 406–413.
Rawlings, N.D., Barrett, A.J., 1990. Evolution of proteins of the cystatin superfamily. J. Mol. Evol. 30, 60–71.
Revesz, T., Holton, J.L., Lashley, T., Plant, G., Frangione, B., Rostagno, A., Ghiso, J., 2009. Genetics and molecular pathogenesis of sporadic and hereditary cerebral amyloid angiopathies. Acta Neuropathol. 118, 115–130.
Romhanyi, G., 1971. Selective differentiation between amyloid and connective tissue structures based on the collagen specific topo-optical staining reaction with congo red. Virchows Arch. A Pathol. Pathol. Anat. 354, 209–222.
Rostagno, A., Holton, J.L., Lashley, T., Revesz, T., Ghiso, J., 2010. Cerebral amyloidosis: amyloid subunits, mutants and phenotypes. Cell. Mol. Life Sci. 67, 581–600.
Sastre, M., Calero, M., Pawlik, M., Mathews, P.M., Kumar, A., Danilov, V., Schmidt, S.D., Nixon, R.A., Frangione, B., Levy, E., 2004. Binding of cystatin C to Alzheimer's amyloid beta inhibits in vitro amyloid fibril formation. Neurobiol. Aging 25, 1033–1043.
Savitsky, A., Golay, M.J.E., 1964. Smoothing and differentiation of data by simplified least-squares procedures. Anal. Chem. 36, 1627–1639.
Sawaya, M.R., Sambashivan, S., Nelson, R., Ivanova, M.I., Sievers, S.A., Apostol, M.I., Thompson, M.J., Balbirnie, M., Wiltzius, J.J., McFarlane, H.T., Madsen, A.O., Riekel, C., Eisenberg, D., 2007. Atomic structures of amyloid cross-beta spines reveal varied steric zippers. Nature 447, 453–457.
Sipe, J.D., Benson, M.D., Buxbaum, J.N., Ikeda, S., Merlini, G., Saraiva, M.J., Westermark, P., 2012. Amyloid fibril protein nomenclature: 2012 recommendations from the Nomenclature Committee of the International Society of Amyloidosis. Amyloid 19, 167–170.
Spodzieja, M., Rafalik, M., Szymanska, A., Kolodziejczyk, A.S., Czaplewska, P., 2013. Interaction of serum amyloid A with human cystatin C – assessment of amino acid residues crucial for hCC-SAA formation (part II). J. Mol. Recognit. 26, 415–425.
Spodzieja, M., Szymanska, A., Kolodziejczyk, A., Pradzinska, M., Maszota, M., Stefanowicz, P., Szewczuk, Z., Grubb, A., Czaplewska, P., 2012. Interaction of serum amyloid A with human cystatin C – identification of binding sites. J. Mol. Recognit. 25, 513–524.
Sunde, M., Blake, C., 1997. The structure of amyloid fibrils by electron microscopy and X-ray diffraction. Adv. Protein Chem. 50, 123–159.

Surewicz, W.K., Mantsch, H.H., Chapman, D., 1993. Determination of protein secondary structure by Fourier transform infrared spectroscopy: a critical assessment. Biochemistry 32, 389–394.
Szymanska, A., Radulska, A., Czaplewska, P., Grubb, A., Grzonka, Z., Rodziewicz-Motowidlo, S., 2009. Governing the monomer-dimer ratio of human cystatin c by single amino acid substitution in the hinge region. Acta Biochim. Pol. 56, 455–463.
Teng, P.K., Eisenberg, D., 2009. Short protein segments can drive a non-fibrillizing protein into the amyloid state. Protein Eng. Des. Sel. 22, 531–536.
Tenidis, K., Waldner, M., Bernhagen, J., Fischle, W., Bergmann, M., Weber, M., Merkle, M.L., Voelter, W., Brunner, H., Kapurniotu, A., 2000. Identification of a penta- and hexapeptide of islet amyloid polypeptide (IAPP) with amyloidogenic and cytotoxic properties. J. Mol. Biol. 295, 1055–1071.
Tian, X., Maftei, M., Kohlmann, M., Allinquant, B., Przybylski, M., 2007. Differential epitope identification of antibodies against intracellular domains of Alzheimer's amyloid precursor protein using high resolution affinity-mass spectrometry. Subcell. Biochem. 43, 339–354.
Tremmel, S., Beyermann, M., Oschkinat, H., Bienert, M., Naumann, D., Fabian, H., 2005. 13C-labeled tyrosine residues as local IR probes for monitoring conformational changes in peptides and proteins. Angew. Chem. Int. Ed. Engl. 44, 4631–4635.
Tsiolaki, P.L., Hamodrakas, S.J., Iconomidou, V.A., 2015. The pentapeptide LQVVR plays a pivotal role in human cystatin C fibrillization. FEBS Lett. 589, 159–164.
Tsolis, A.C., Papandreou, N.C., Iconomidou, V.A., Hamodrakas, S.J., 2013. A consensus method for the prediction of 'aggregation-prone' peptides in globular proteins. PLoS ONE 8, e54175.
Turk, V., Bode, W., 1991. The cystatins: protein inhibitors of cysteine proteinases. FEBS Lett. 285, 213–219.
Valenti, L.E., Paci, M.B., De Pauli, C.P., Giacomelli, C.E., 2011. Infrared study of trifluoroacetic acid unpurified synthetic peptides in aqueous solution: trifluoroacetic acid removal and band assignment. Anal. Biochem. 410, 118–123.
Zerovnik, E., 2009. The emerging role of cystatins in Alzheimer's disease. BioEssays 31, 597–599.
Zerovnik, E., Staniforth, R.A., Turk, D., 2010. Amyloid fibril formation by human stefins: structure, mechanism & putative functions. Biochimie 92, 1597–1607.
Zerovnik, E., Stoka, V., Mirtic, A., Guncar, G., Grdadolnik, J., Staniforth, R.A., Turk, D., Turk, V., 2011. Mechanisms of amyloid fibril formation – focus on domain-swapping. FEBS J. 278, 2263–2282.

Contents lists available at ScienceDirect

Journal of Structural Biology

journal homepage: www.elsevier.com/locate/yjsbi

Volume 191, Issue 3, September 2015

CONTENTS

Regular Articles

Continued

Front Cover: A suggested model of stacked octamers for human Cystatin C fibrillization implicates two important "aggregation-prone" hotspots, *CysC1* (^{47}LQVVR^{51}, red) and *CysC2* (^{56}IVAGVNYFLD^{65}, blue).

For a full and complete Guide for Authors, please go to: http://www.elsevier.com/locate/yjsbi

Abstracted/indexed in Biological Abstracts, Chemical Abstracts, Current Contents/Life Sciences, EMBASE, EMBiology, Excerpta Medica, MEDLINE® Research Alert, SCISEARCH, Science Citation Index. Also covered in the citation database Scopus®. Full text available on ScienceDirect®

1047-8477(201509)191:3;1-1

Technical Notes